HHS Public Access

Author manuscript

Cell Rep. Author manuscript; available in PMC 2024 September 03.

Published in final edited form as:

Cell Rep. 2024 July 23; 43(7): 114459. doi:10.1016/j.celrep.2024.114459.

SART3 reads methylarginine-marked glycine- and arginine-rich motifs

Yalong Wang[1], **Jujun Zhou**[1], **Wei He**[1], **Rongjie Fu**[1], **Leilei Shi**[1], **Ngoc Khoi Dang**[1], **Bin Liu**[1], **Han Xu**[1], **Xiaodong Cheng**[1], **Mark T. Bedford**[1,2,*]

[1]Department of Epigenetics & Molecular Carcinogenesis, The University of Texas MD Anderson Cancer Center, Houston, TX 77030, USA

[2]Lead contact

SUMMARY

Glycine- and arginine-rich (GAR) motifs, commonly found in RNA-binding and -processing proteins, can be symmetrically (SDMA) or asymmetrically (ADMA) dimethylated at the arginine residue by protein arginine methyltransferases. Arginine-methylated protein motifs are usually read by Tudor domain-containing proteins. Here, using a GFP-Trap, we identify a non-Tudor domain protein, squamous cell carcinoma antigen recognized by T cells 3 (SART3), as a reader for SDMA-marked GAR motifs. Structural analysis and mutagenesis of SART3 show that aromatic residues lining a groove between two adjacent aromatic-rich half-a-tetratricopeptide (HAT) repeat domains are essential for SART3 to recognize and bind to SDMA-marked GAR motif peptides, as well as for the interaction between SART3 and the GAR-motif-containing proteins fibrillarin and coilin. Further, we show that the loss of this reader ability affects RNA splicing. Overall, our findings broaden the range of potential SDMA readers to include HAT domains.

In brief

Using a composite arginine methylation substrate, Wang et al. identify SART3 as a “reader” of symmetrically dimethylated arginine (SDMA) motifs. This binding is mediated by a groove formed between two adjacent aromatic-rich half-a-tetratricopeptide (HAT) repeat domains. The integrity of this methyl-dependent interaction is required for normal splicing.

Graphical Abstract

*Correspondence: mtbedford@mdanderson.org.

AUTHOR CONTRIBUTIONS

Experimental design, Y.W.; execution, Y.W.; data analysis, Y.W.; manuscript preparation, Y.W. and M.T.B.; ITC experiments, J.Z.; data interpretation, L.S., R.F., W.H., H.X., and M.T.B.; bioinformatic analysis, B.L. and N.K.D.; structural modeling & editing, X.C.; supervision of the research, M.T.B.

DECLARATION OF INTERESTS

M.T.B. is the co-founder of EpiCypher.

SUPPLEMENTAL INFORMATION

Supplemental information can be found online at https://doi.org/10.1016/j.celrep.2024.114459.

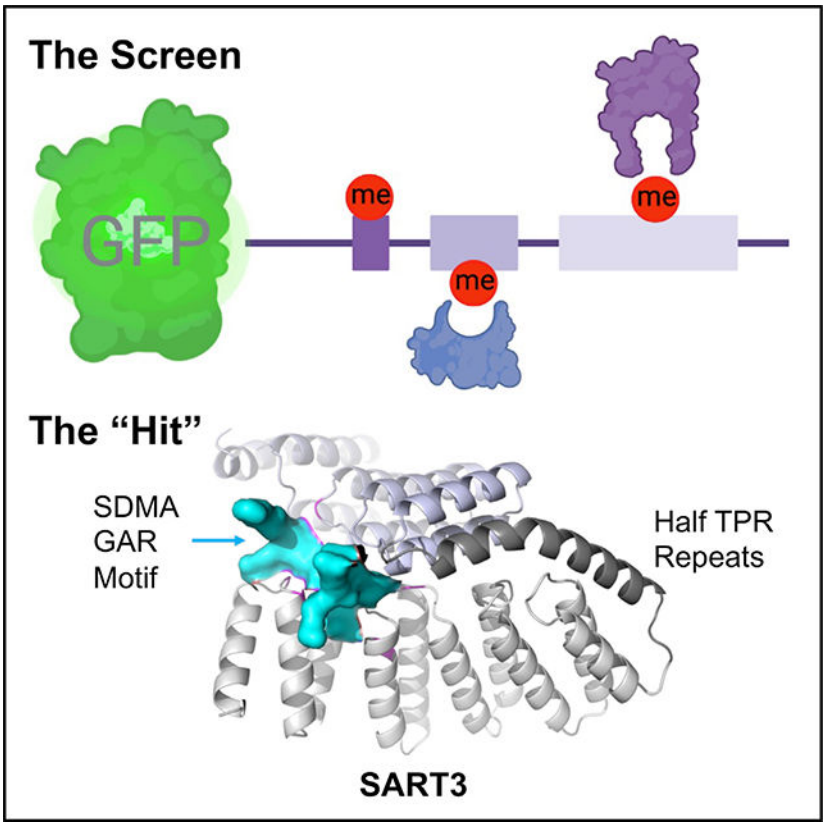

INTRODUCTION

Arginine methylation is an important post-translational modification involved in diverse biological processes.[1] There are three distinct types of methylated arginine residues: asymmetric dimethylarginine (ADMA), symmetric dimethylarginine (SDMA), and mono-methylarginine (MMA). Arginine methylation is catalyzed by the family of protein arginine methyltransferases (PRMTs), of which there are nine members in mammals.[2] PRMTs are classified into three types according to their catalytic activity. Type I PRMTs catalyze the deposition of ADMA marks, type II PRMTs catalyze the deposition of SDMA marks, and a lone type III PRMT is responsible for MMA marks. The three forms of arginine methylation are abundant, and 0.5%–4% of all arginine residues are methylated in mammalian cells.[3]

Identifying the substrates of the different PRMTs is the first step in elucidating the function of arginine methylation. Many approaches to substrate identification have been taken, including protein array screens,[4] small-pool screens,[5] and pan-arginine methylation-specific antibodies[6] that can serve as enrichment reagents in mass spectrometry experiments.[7–9] The arginine-methylated proteome is now well cataloged.[10] Most PRMTs methylate glycine- and arginine-rich (GAR) motifs within their substrates, including the highly active type I and II enzymes PRMT1 and PRMT5, respectively.[8,11] Indeed, a recent proteomic study reports that about 70% of arginine methylation occurs within GAR motifs.[12] GAR motifs are typically composed of either RGRG or RGGRGG repeats.[11] Importantly, the same GAR motif within a protein can be a shared substrate of both PRMT1 and PRMT5.[8,13]

Direct consequences of arginine methylation include the regulation of (1) adjacent post-translational modification events, (2) subcellular protein localization, (3) phase separation, and (4) protein-protein interactions.[1,2,14,15] Arginine-methylated motifs can serve as docking sites for effector proteins that "read" either an SDMA or ADMA motif on a substrate.[14,16] This reader function is often mediated through Tudor domains. There are roughly 30 Tudor domain-containing proteins in humans, many of which are effectors for methyllysine or methylarginine marks.[16,17] For example, the Tudor domains of SMN, SPF30/SMNDC1, and SND1 are well-characterized SDMA readers, whereas the Tudor domain of TDRD3 is a major ADMA reader.[16] A crucial element of Tudor domains that recognize methyl marks is that the domain forms an aromatic-binding cage, created by several aromatic residues that interact with the methyl mark through cation-π interactions.[18] Although methyllysine motifs are recognized by at least eight different domain types,[17,19,20] Tudors are the only identified domain family known to recognize methylarginine marks.[16] This paucity of methylarginine mark effectors prompted us to screen for additional readers.

Here, we identify squamous cell carcinoma antigen recognized by T cells 3 (SART3[21]; also called Tip110) as an SDMA effector protein. SART3 is a multifunctional protein that is involved in U4/U6 small nuclear ribonucleoprotein (snRNP) recycling,[22] RNA splicing,[23,24] viral and host gene expression,[25,26] and H2B histone deubiquitylation.[27] The N-terminal half of SART3 is composed of recurrent elements related to tetratricopeptide repeats (TPRs), termed half-a-tetratricopeptide (HAT) repeats.[28] This region of SART3 is further organized into HAT-N (5 repeats) and HAT-C (7 repeats) subdomains.[29] We identify the HAT repeat region of SART3 as a reader of methylarginine-marked GAR motifs, raising the possibility that other proteins with HAT repeats or TPRs could be effectors of methyl marks.

RESULTS

SART3 interacts with a methylated arginine motif

A GFP-Trap approach (developed by ChromoTek), using nanobody-based reagents, is an efficient way to identify protein-protein interactions in cells.[30] Here, we used a GFP-Trap to identify additional effectors of methylarginine marks. We created a chimeric protein composed of the arginine-methylated regions from three different proteins: the GAR region (residues 1–68) of fibrillarin that can be both SDMA and ADMA modified[31] and regions of PABPC1 (residues 429–472) and FAM168B (residues 68–107) that represent CARM1 substrates[4] (Figure S1A). We refer to this chimeric protein as RMET for arginine methylation (Rme) effector trap (Figure 1A). The RMET plasmid vector was transiently expressed in HEK293T human embryonic kidney cells in either the presence or absence of one of four inhibitors: a global methyltransferase inhibitor (AdOx),[32] a type I PRMT inhibitor (MS023),[33] a CARM1 inhibitor (TP064),[34] or a PRMT5 inhibitor (EPZ015666).[35] Inhibitor-induced change of arginine methylation at the three regions in RMET was confirmed by immunoblot using methyl-specific antibodies (Figure S1B). This result showed that RMET undergoes arginine methylation when expressed in cells.

To identify methylarginine effectors of RMET, we performed a GFP-Trap purification in the presence and absence of AdOx (Figure 1A) and identified the associated proteins using mass-spectrometry-based label-free quantification. We recovered two known methyl-

dependent GAR-motif readers (SND1 and SMN) that were selectively enriched as RMET binders, exclusively in cells that were not treated with AdOx (Figure 1B; Table S1), which served as positive controls for the experiment.[16] We also recovered PRMT1, PRMT5, and PRMT5-interacting proteins (MEP50 and RIOK1) as relatively enriched proteins in cells treated with AdOx (i.e., monomethylated RMET), intimating that these PRMTs only efficiently disengage from their substrates after dimethylation has occurred. Finally, like SND1 and SMN, SART3 exhibited significant enrichment in the protein complex from untreated cells compared to treated cells (peptide count: 38 to 0). This finding suggests that SART3 may be an effector of dimethylarginine motifs.

SART3 co-localizes with both coilin and fibrillarin,[36,37] two proteins with long and very well-characterized GAR motifs that serve as major PRMT substrates.[11,38–40] To assess the binding of ectopically expressed RMET to endogenous SART3, SND1, and SMN, we transiently transfected GFP-RMET into HEK293T cells and performed co-immunoprecipitation (coIP) experiments and western blot analysis. All three proteins bound to RMET, but the binding decreased with AdOx treatment, indicating that the interactions are dimethylation dependent (Figure S1C). Furthermore, with the substitution of lysines for an arginine residue in RMET (RMET-R to RMET-K), the interaction between SART3 and RMET-K was abolished, suggesting that the interaction, whether direct or indirect, requires arginine residues (Figure S1D).

SART3 directly binds symmetrically methylated GAR motifs through its HAT repeat domain

SART3 contains several distinct domains, including HAT repeats and RNA recognition motif (RRM) domains. The HAT repeat domains have a repetitive pattern, characterized by aromatic residues with a conserved spacing. Given that all reported arginine methylation readers utilize aromatic residues to recognize arginine methylation,[16] we hypothesized that the HAT repeats of SART3 might read arginine methylation marks. To test this possibility, we performed a far-western analysis using cell lysates from HEK293T cells expressing (1) GFP alone, (2) GFP-RMET, (3) GFP-RMET and treated with AdOx, and (4) GFP-RMET-K, which were probed with a GST-SART3(HAT) recombinant protein, followed by anti-GST antibody. We found that the GST-SART3(HAT) signal was enriched on wild-type (WT) RMET extracts but not AdOx-treated or RMET-K extracts (Figure 1C), supporting the hypothesis that the HAT repeats of SART3 directly recognize the arginine-methylated motif in RMET.

To determine whether the methyl-dependent interaction between SART3 and RMET is driven by SDMA or ADMA, we performed pull-down assays of glutathione S-transferase (GST) fusion proteins with biotinylated, synthetic GAR motif peptides representing the fibrillarin GAR motif (utilized in the cloning of RMET). The biotinylated peptides used in the pull-down assay were synthesized as unmethylated, ADMA modified, or SDMA modified. Notably, only the SDMA-modified peptide pulled down GST-SART3(HAT) (Figure 1D, top). As controls, GST-TDRD3 interacted strongly with the ADMA-methylated peptide and GST-SMN interacted with the SDMA-methylated peptide (Figure 1D, bottom two images). In addition, the SDMA-modified GAR peptide of coilin also directly binds to GST-SART3(HAT). The GAR peptide of coilin harbors five arginine residues, and we

generated two methylated peptides, with either the first three (1–3) or last three residues (3–5) methylated. The peptide harboring SDMA modifications of the last three arginine residues (3–5) displayed a strong interaction with GST-SART3 (Figure 1E, top), and the interaction was maintained under stringent conditions of a radio-immunoprecipitation assay (RIPA) buffer (Figure 1E, bottom). Isothermal titration calorimetry (ITC) experiments determined that the GST-SART3 HAT repeats bind the coilin SDMA peptides with an equilibrium dissociation constant (K_D) of 15–18 μM (Figure S1E).

The complete HAT repeat domain of SART3 is needed to engage a methylated GAR motif

SART3 possesses twelve HAT repeats at its N terminus and two RRMs at its C terminus (Figure 2A). The structure of the N-terminal HAT repeats has been elucidated,[29] showing that they configure two subdomains (HAT-N and HAT-C), with HAT-C facilitating dimer formation (Figure 2B). Utilizing four GST fusion proteins bearing all SART3 HAT repeats (N + C), only HAT-N, only HAT-C, or the two RRMs, we performed interaction mapping experiments and found that arginine-methylated GAR peptides derived from fibrillarin or coilin interacted exclusively with GST fusions bearing the full complement of HAT subdomains (N + C) (Figure 2A). Interestingly, structural analysis of SART3 identified a groove that forms between the HAT-N and HAT-C subdomains[29] (green and teal in Figure 2B), creating a potential methylarginine binding site that incorporates aromatic residues from both subdomains.

To further explore this groove for potential interactions with methyl arginine, we substituted alanine for ten aromatic residues situated in, near, or away from the groove. Specifically, Y110, Y112, F142, and Y180 of HAT-N and W377 of HAT-C are surface exposed along the groove, and W149 of HAT-N is buried within a cage structure (Figure 2C). Additionally, Y313, F411, Y417, and W421 of HAT-C are buried and located away from the groove. We tested these GST-SART3 mutants in pull-down assays using SDMA-modified GAR motif peptides (Figure 2D). We found four aromatic residues, three in HAT-N (Y112, F142, and Y180) and one in HAT-C (W377) that, when mutated, exhibited a complete loss of interaction with the two modified GAR peptides (Figure 2D). The Y110A mutant also showed reduced interactions with both peptides. W149A, situated at the bottom of an aromatic cage, exhibited a reduced interaction with the fibrillarin peptide but no interaction with the coilin peptide. Conversely, alanine substitutions at four distant aromatic HAT-C residues had no effect on the interaction with the fibrillarin peptide, and only W421A had an effect (a weakened interaction with the coilin peptide). Together, this evidence is consistent with GST-SART3 relying on a cluster of aromatic residues from both sides of the groove to read SDMA marks, making both HAT-N and HAT-C essential for binding. Notably, the cluster of five aromatic residues of SART3 (Y112, F142, W149, Y180, and W377) are conserved in vertebrates but not *Caenorhabditis elegans*. Indeed, we found that SART3 HAT regions from six different vertebrate species, but not *C. elegans*, selectively bound to the coilin-SDMA peptide (Figures S2A and S2B).

Consistent with our observation that SART3 selectively interacts with SDMA-modified GAR motifs (Figures 1D and 1E), inhibition of PRMT5 with EPZ015666 in HEK293T cells reduced the interaction between GFP-SART3 and endogenous fibrillarin and coilin

in IP experiments (Figures S2C and S2D). Importantly, this reduced interaction was not observed when PRMT1 was inhibited with MS023. Notably, no dramatic inhibitor effect was observed on the interaction between SART3 and its binding partners AGO1, La/SSB, SAP145, and USP4/15.[29,41–43] Thus, blocking SDMA methylation of endogenous fibrillarin and coilin by inhibiting PRMT5 results in impaired binding to ectopically expressed SART3. We have modeled the binding of the human SART3 HAT repeats to the unmethylated GAR peptides using AlphaFold-Multimer. Both fibrillarin (Figures S3A–S3C) and coilin (Figures S3D–S3F) peptides preferentially associate in the groove between the HAT repeat regions of SART3 in a manner that could present the methylated arginine residues to the aromatic cages located at the bottom of the groove (Figure 2C).

To determine whether the surface aromatic residues in the groove between HAT-N and HAT-C that interact with SDMA GAR are critical for interaction with coilin and fibrillarin in human cells, we transiently overexpressed both WT and mutant forms of GFP-SART3 in HeLa cells and performed IP experiments. While WT SART3 co-precipitated both coilin and fibrillarin, the SART3 mutants (Y112A, F142A, Y180A, and W377A) demonstrated a reduced ability to co-precipitate these proteins (Figure S4A). The residual binding between the SART3 mutants and fibrillarin/coilin likely results from SART3 dimer formation between the transiently expressed SART3 mutants and endogenous SART3. To address this issue, we knocked out SART3 in HeLa cells using CRISPR-Cas9 before stably reintroducing either GFP-tagged WT SART3 or GFP-tagged SART3 mutants. Both knockout and restoration efficiencies were validated through western blot analysis (Figure 3A). coIP experiments showed that although reintroduced WT SART3 interacted with both coilin and fibrillarin, the reintroduced SART3 mutants (Y112A of HAT-N and W377A of HAT-C) completely disrupted the interaction (Figure 3B).

SART3 methylarginine effector mutants exhibit aberrant splicing

To better define the functional importance of the SART3 SDMA binding domain, we used a GFP-Trap approach to identify proteins that no longer complex with SART3 when its methyl-reader ability is compromised. We transiently transfected HeLa cells with a GFP empty vector control, GFP-SART3 WT, GFP-SART3(Y112A), or GFP-SART3(W377A). Binding partners were identified by mass-spectrometry-based label-free quantification and compared between WT and mutant SART3 proteins to identify potential binding partners (apart from coilin and fibrillarin) that complex with SART3 in a methyl-dependent manner. Kyoto Encyclopedia of Genes and Genomes Pathway analysis showed that those proteins that lost interaction with the SART3 mutants are significantly enriched in the spliceosomal pathway (Figure S4B; Table S2). Further, the lost interactions strongly overlapped between the two SART3 mutants (Figure S4C). These data indicate that SART3, as a methylarginine effector, likely helps regulate RNA splicing. Subsequent coIP experiments using the CRISPR knockout/rescued HeLa cell line set confirmed that representative spliceosomal proteins including EFTUD2, SNRNP200, SART1, PRPF6, and SNRPB exhibited reduced interactions with the two SART3 mutants compared with WT SART3 (Figure 3C). Moreover, treatment with the PRMT5 inhibitor EPZ015666 also inhibits the interaction between SART3 and the representative spliceosomal proteins (Figure S4D).

To determine the potential role of the methylarginine effector function of SART3 in splicing and identify candidate genes that are aberrantly spliced in the absence of SART3's reader function, we performed RNA sequencing (RNA-seq) (150-nt paired-end sequencing) using the rescued HeLa cell line set depicted in Figure 3A. With the consideration of sample variation and read coverage for splicing junctions, three sets of biological replicates were prepared for RNA-seq with minimum 130 million reads for each of the 9 samples (3 × WT rescue; 3 × W337A rescue; 3 × Y112A rescue), and the mapped BAM files were used as inputs for replicate multivariante analysis of transcript splicing (rMATS)[44] to detect differential alternative splicing events. We observed a broad spectrum of changes in splicing in SART3 mutants, including alteration in the exon skipping rate, retained introns, alternative 5′ or 3′ splice site usage, and mutually exclusive exons. Similar rates of changes for these splicing categories were observed for both analyzed mutants, with skipped exons accounting for ~65% of the splicing alterations (Figure S5A). There is >40% overlapped site-specific exon usage within each of the five different splicing categories between the two SART3 mutants. Upon examining the Gene Ontology (GO) of the skipped exon events, we found that the GO terms were remarkably similar in both SART3 mutant samples (Figure S5B). We also performed differential expression analysis on this RNA-seq data, which showed a very limited number of differentially expressed genes in both SART3 mutants when compared with the WT (Figure S5C; Table S3). Additionally, the magnitude of expression change in these genes was minimal. These findings suggest that the mutations in SART3 primarily influence its role in RNA splicing rather than robustly altering gene expression.

Two examples of the mixture of isoforms (MISO) output landscape, displayed as Sashimi plots, show the RNA-seq read coverage across the genes for transmembrane protein 255B (*TMEM255B*) and microtubule-associated tyrosine carboxypeptidase 2 (*MATCAP2/KIAA0895*) from the WT-rescued control and the W337A- and Y112A-rescued HeLa cells (Figure 3D). The rescued mutant lines displayed reduced exon skipping (exon 4 for transcript ENST00000375353.5) for *TMEM255B*, while an inclusion event was decreased (exon 3 for transcript ENST00000440378.6) for *KIAA0895* (Figure 3D). To validate the alternative splicing events called by MISO, RT-PCR was performed using primers located within the exons flanking the impacted exon of these two genes. In both cases, the inclusion/exclusion ratio was altered ~2-fold when SART3 methylarginine effector function was blocked (Figure 3E). Together, these data indicate that the methylarginine effector function of SART3 is involved in regulating RNA splicing.

DISCUSSION

The PRMT5-MEP50-pICln complex methylates Sm proteins, which are critical for the maturation of small nuclear ribonucleo-proteins and spliceosome assembly.[45–47] Arginine methylation plays a critical role in the regulation of splicing and splicing factor performance, with the Tudor domains of SMN and its paralog SMNDC1 functioning as effectors of methylated Sm proteins.[48] SMN and SMNDC1 display distinct subcellular localization patterns and are both involved in the regulation of phase-separated, membraneless organelles.[14,49] Interestingly, SMN and SART3 do not generally co-localize but are found in two overlapping nuclear biomolecular condensates, Gemini bodies (gems) and Cajal bodies,

respectively.[15,50] SART3 is a Cajal body scaffolding protein and is required for the induction of Cajal body formation.[36] This raises the possibility that the SDMA effector properties of SART3 are important for the integrity of Cajal bodies. Indeed, work performed over 20 years ago showed that the arginine methylation of coilin regulates Cajal body formation.[51] Our findings support a modality for PRMT5 regulation of splicing that is mediated by SART3, independent of SMN and SMNDC1.

The HAT repeat region of SART3 is an SDMA reader, which raises the possibility that other HAT/TPR-containing proteins harbor methyl-reading abilities. Indeed, the 34-amino-acid-long TPR, characterized by a high content of aromatic residues with a consensus of $W_4G_8Y_{11}G_{15}Y_{17}A_{20}Y_{24}A_{27}P_{32}$,[52] seems predisposed to form aromatic grooves for methyl reading. HATs have a repeating pattern of three aromatic residues,[53,54] and there are over 300 different human proteins with TPR motifs and 11 proteins with HAT motifs in the EMBL SMART database. Of particular interest are TPR-motif-containing proteins with links to epigenetic regulation or splicing, including KDM6A (UTX) and KDM6B (UTY), OGT, PRMT9 and Gemin5. It is possible that the TPR/HAT-containing proteins may represent an emerging family of reads for methylated protein motifs.

The SDMA-binding region of SART3 diverges from the usual formation of a typical aromatic cage, designed for accommodating a single methylated residue. Instead, SART3's ability to recognize SDMA hinges on a cluster of aromatic residues arranged along a groove created between the HAT-N and HAT-C folds. This unique structure potentially allows for the accommodation of longer peptides with multiple methylated residues (Figure 2C). The ability of the distal regions of a protein to assemble into aromatic-rich regions for enhanced methyl-reader activity has recently been demonstrated for the methyllysine effector protein PHF2.[55] These two studies (SART3 and PHF2) set a precedent for the generation of methyl-effector interfaces that are generated by protein folding or protein complex assembly, as opposed to an isolated domain harboring the activity intrinsically.

Limitations of the study

In this study, we identified SART3 as a reader of SDMA marks. We show that this reader function is key for the ability of SART3 to bind both coilin and fibrillarin in cells. However, we do not know which methyl-dependent interaction(s) of SART3 drive the splicing defects we see in the SART3 aromatic residue mutants. Indeed, it is very likely that SART3 binds additional SDMA-modified proteins apart from coilin and fibrillarin. We have not evaluated the ability of SART3 to bind mono-methylated arginine motifs. Structural studies will be valuable to ascertain how multiple methylated residues within a GAR motif engage the aromatic groove in SART3.

STAR★METHODS

RESOURCE AVAILABILITY

Lead contact—Further information and requests for resources and reagents should be directed to and will be fulfilled by the lead contact, Mark T. Bedford (mtbedford@mdanderson.org).

Materials availability—Plasmids, antibodies, and cell lines generated in this study will be available from the lead contact upon request with a completed material transfer agreement.

Data and code availability

- All gene expression data utilized in the study are publicly available, and the GEO accession number is GSE246489. The mass spectrometry proteomics data have been deposited to the ProteomeXchange Consortium via the PRIDE partner repository with the dataset identifier PXD044862 (Maria) and PXD046708 (Bill).
- This paper does not report original code.
- Any additional information required to reanalyze the data reported in this paper is available from the lead contact upon request.

EXPERIMENTAL MODEL AND STUDY PARTICIPANT DETAILS

Cell culture and treatment—HEK293T and HeLa cells were maintained at 37°C in Dulbecco's modified Eagle's medium supplemented with 10% FBS and 1% Antibiotic-Antimycotic. Cells at 80% confluence were transfected with plasmids using lipofectamine 2000. To generate the HeLa SART3 KO cell line, SART3 sgRNA designed using CRISPick (Broad Institute) was subcloned into the LentiCRISPRv2 plasmid. Production of lentivirus was performed in HEK293T cells by co-transfection with pMD2-G, psPAX2 and LentiCRISPRv2 plasmids. Viral supernatant was collected over 2 days. For infection, cells were seeded in a 6-well plate at $5X10^4$ per well. The next day 1mL viral supernatant was added with 10 mg/ml polybrene for 24 h followed by a media change. Blasticidin (10 μg/mL) was added to the culture medium 48 h after infection for HeLa SART3-KO cell line generation. The cells were then plated at a low density (0.5 cell/well) to get well separated colonies. Single SART3-KO clones were manually picked and validated for further experiments. For HeLa SART3 KO cell restoration, different SART3 mutants were generated from WT lenti-Puro-GFP-SART3 by using Q5 site-directed mutagenesis kit (NEB #E0554S). The SART3 plasmids were co-transfected with pMD2-G and psPAX2 into HEK293T for virus production. HeLa cells were infected with the lentivirus, and puromycin (2 μg/mL) was added to the culture medium 48 h after infection to select for stable cells lines with restored SART3 expression. In inhibitor treatments, 25uM AdOx, 1uM MS023, or 10uM EPZ015666 were administered for 3 days before harvesting cell lysates.

METHOD DETAILS

Recombinant protein expression and purification—The DNA sequences of different gene domain regions were synthesized by Biomatik with codon optimization and inserted into pGEX-4T-1 vector backbone. The construct was verified by sequencing and was transformed into *E. coli* BL21. A single colony from the transformation was used to inoculate LB supplemented with 100 mg/mL ampicillin. Expression was induced by adding IPTG to 0.1mM. After 6–12h induction at 18°C, cells were harvested, lysed by sonication and clarified by centrifugation prior to incubation with glutathione Sepharose beads for 4h at 4°C. Then the beads were washed and incubated with fresh glutathione reduced elution buffer for 2–3h at 4°C for protein elution.

Generation of methylarginine antibodies—The details of MMA, ADMA and SDMA antibody generation have been described previously.[6] Briefly, the same antigen structure was used to generate all three types of the antibody, namely N2H-GGRG(dPEG4)GRG(dPEG4)GRG(dPEG4)C-amid. All R residues in the peptide were modified with MMA, ADMA or SDMA depending on the antibody project. The antibodies were produced in rabbits by New England Peptide (NEP). The FAM(ADMA) antibody was raised in rabbits against the human FAM168B peptide sequence QTAVYPVR(me2s)SAYPQQ, which harbors symmetrically methylated arginine residue.

GFP-trap immunoprecipitation and LC-MS—Cells were harvested, washed with ice-cold PBS, and total cell extracts were prepared in mild lysis buffer (10mM Tris/Cl pH 7.5; 150mM NaCl; 0.5mM EDTA; 0.5% NP-40) and protease inhibitor cocktail. After sonication, insoluble materials were removed by centrifugation. Whole cell lysates were incubated with GFP-trap agarose for 2 h at 4°C. Then the agarose was washed, and the bound proteins were eluted and separated on polyacrylamide gels for western blot analysis or for LC-MS analysis. For LC-MS analysis, samples were cut from the gel and the protein was identified with LC-MS/MS on a Thermo Ultimate 3000 RSLCnano UPLC in-line with an Orbitrap Fusion at the Proteomics Facility at UT Austin. Proteins were identified with Proteome Discoverer 2.2 (Thermo) using the Sequest HT search engine, with 10 ppm mass tolerance for the MS at 0.6 Da for the MS/MS. Identifications were validated with Scaffold 5 (Proteome Software) using protein threshold of 1% FDR for 2 peptides at peptide threshold of 0.1% FDR.

Co-immunoprecipitation and western blotting—Cells were harvested, washed with ice-cold PBS, and total cell extracts were prepared in mild lysis buffer (10mM Tris/Cl pH 7.5; 150mM NaCl; 0.5mM EDTA; 0.5% NP-40) and protease inhibitor cocktail. GFP antibody was incubated with Protein A/G beads (Thermo Scientific) for 2h at 4°C, washed three times with lysis buffer, followed by incubation with the cell lysates for 2h at 4°C. Then the beads were washed three times with lysis buffer and boiled in loading buffer to elute the bounded proteins. The cell extracts or immunoprecipitated samples were separated by SDS-PAGE and transferred onto PVDF membranes. Blots were blocked in PBS containing 5% non-fat dry milk, then incubated with the appropriate primary antibody in the blocking buffer overnight at 4°C. The blots were then washed with PBST (PBS with 0.05% tween 20) and probed with an HRP-labelled secondary antibody for 1h at room temperature. After washing three times with PBST, the membranes were incubated with ECL reagent and the signal was detected on X-ray film.

Far-western blotting—GFP-RMET or GFP-Coilin proteins were immunoprecipitated from HEK293T cells, separated by SDS-PAGE, and transferred onto PVDF membrane. Blots were blocked in 5% non-fat milk and then incubated with 5 μg/mL GST-tagged protein in the blocking buffer for 1 h at room temperature. The blots were then washed and probed with an anti-GST antibody and incubated with an HRP-labeled secondary antibody for detection by chemiluminescence. The blots were then washed with PBST (PBS with 0.05% tween 20) and probed with an HRP-labelled secondary antibody for 1h at room temperature.

After washing three times with PBST, the membranes were incubated with ECL reagent and the signal was detected on X-ray film.

Peptide pull-downs—The streptavidin beads were pre-washed with cell lysis buffer, before incubation with biotinylated peptides in 500 μL mild lysis buffer for 1h at 4°C, with rocking for conjugation. The conjugated peptide-bead complex was then washed 3 times in mild buffer and incubated with 2 μg GST-tagged proteins for 1h at 4°C with rocking. After incubation, the bound proteins were eluted for western blot analysis. Peptides used in this study were:

GAR-un peptide (unmethylated) FBL: GGRGRGGGFRGRGRGGGG-Biotin;

GAR-Rme2a peptide (ADMA):
GG[Rme2a]G[Rme2a]GGGF[Rme2a]G[Rme2a]G[Rme2a]GGGG-Biotin;

GAR-Rme2s peptide (SDMA):
GG[Rme2s]G[Rme2s]GGGF[Rme2s]G[Rme2s]G[Rme2s]GGGG-Biotin;

Coilin-un peptide (unmethylated): Biotin-AKGRGMRGRGRGRGHP-Amide;

Coilin-(1–3) Rme2s peptide (SDMA): Biotin-
AKG[Rme2s]GM[Rme2s]G[Rme2s]GRGRGHP-Amide;

Coilin -(3–5) Rme2s peptide (SDMA): Biotin-
AKGRGMRG[Rme2s]G[Rme2s]G[Rme2s]GHP-Amide.

AlphaFold modeling—The interaction between human SART3 (residues 94–611) and GAR peptide or colin peptide, (GGRGRGGGFRGRGRGGGG) or (AKGRGMRGRGRGRGHP) respectively, was modeled using AlphaFold-Multimer. The default settings were employed by treating SART3 and peptide as a heterodimer. The predicted complex models were visualized by PyMOL (version 2.5.2).

RNA sequencing and splicing analysis—Total RNA was extracted from HeLa cells using a RNeasy kit (QIAGEN, 74106). RNA samples were sent to MedGenome for sequencing. cDNA libraries were made using an Illumina TruSeq stranded mRNA kit and sequencing was performed using a NovaSeq (PE150) machine. Paired-end (150-nt) sequencing was performed with minimum 130 million reads for each of the 9 samples (3 × WT rescue; 3 × W337A rescue; 3 × Y112A rescue). The FASTQ files of 3 conditions (WT rescued, W377A rescued and Y112A rescued) in three biological replicates were checked by FastQC. The low-quality bases and the adaptors were removed by TrimGalore. After that, the clean data was mapped to human reference genome GRCh38.p14[3] and annotated (version 42) using Tophat2 aligner. The mapped bam files for three replicates were used as inputs for rMATS[44] to detect differential alternative splicing events. We used the default setting from the rMATS to define a significant splicing event. The false discovery rate was set as FDR ≤ 0.05. The selected alternative splicing events from output files of rMATS splicing were then visualized as Sashimi plot by using a bioinformatics tool rmats2sashimiplot (https://github.com/Xinglab/rmats2sashimiplot). The

package “rmats2sashimiplot” is using mixture-of-isoforms (MISO) software[56,57] as its backend.

PCR for splicing analysis—Total RNA was extracted from HeLa cells using a RNeasy kit (QIAGEN, 74106). cDNA was prepared using iScript cDNA Synthesis Kit (Bio-rad, #1708891). PCR products were separated on a 2% agarose gel. Primer information is contained in Supplemental Information, Table S4.

Isothermal titration calorimetry—Isothermal Titration Calorimetry (ITC) experiments were conducted using a MicroCal PEAQ-ITC automated system (Malvern) at 25°C. Reference power was maintained at 8 μcal/s. The experiments were carried out in an ITC buffer containing 20 mM TRIS-HCl (pH 8.0), 0.5 mM TCEP, 5% glycerol, and 50 mM NaCl. Peptides were prepared at a concentration of 800 μM in the same ITC buffer. Nineteen injections of peptides were performed, starting with an initial injection of 0.2 μL, followed by 18 injections of 2 μL each. These peptides were titrated into a solution of 20 μM SART3 protein. ITC data analysis was performed by fitting the data using a ‘one site’ binding model with the offset subtracted. The binding constants were calculated using the ITC analysis module provided by the manufacturer.

QUANTIFICATION AND STATISTICAL ANALYSIS

Two-tailed Ratio-paired t-tests, or Student’s t-tests, were performed using Graphpad Prism, as indicated. Information on the number of experimental replicates is included in the relevant figure legend.

Supplementary Material

Refer to Web version on PubMed Central for supplementary material.

ACKNOWLEDGMENTS

This work was supported by grants to M.T.B. (NIH R35GM153387) and X.C. (NIH R35GM134744 and CPRIT RR160029). X.C. is a CPRIT Scholar in Cancer Research. We thank Maria Person (RRID:SCR021728) and William Russell (CPRIT RP190682) for assistance with the mass spectrometry, Shaobo Dai and John Horton for crystallization efforts, and Briana Dennehey for proof-reading and edits.

REFERENCES

1. Blanc RS, and Richard S (2017). Arginine Methylation: The Coming of Age. Mol. Cell. 65, 8–24. 10.1016/j.molcel.2016.11.003. [PubMed: 28061334]
2. Bedford MT, and Clarke SG (2009). Protein arginine methylation in mammals: who, what, and why. Mol. Cell. 33, 1–13. 10.1016/j.molcel.2008.12.013. [PubMed: 19150423]
3. Maron MI, Lehman SM, Gayatri S, DeAngelo JD, Hegde S, Lorton BM, Sun Y, Bai DL, Sidoli S, Gupta V, et al. (2021). Independent transcriptomic and proteomic regulation by type I and II protein arginine methyltransferases. iScience 24, 102971. 10.1016/j.isci.2021.102971. [PubMed: 34505004]
4. Lee J, and Bedford MT (2002). PABP1 identified as an arginine methyltransferase substrate using high-density protein arrays. EMBO Rep. 3, 268–273. 10.1093/embo-reports/kvf052. [PubMed: 11850402]
5. Cheng D, Côté J, Shaaban S, and Bedford MT (2007). The arginine methyltransferase CARM1 regulates the coupling of transcription and mRNA processing. Mol. Cell. 25, 71–83. 10.1016/j.molcel.2006.11.019. [PubMed: 17218272]

6. Wang Y, Person MD, and Bedford MT (2022). Pan-methylarginine antibody generation using PEG linked GAR motifs as antigens. Methods 200, 80–86. 10.1016/j.ymeth.2021.06.005. [PubMed: 34107353]
7. Guo A, Gu H, Zhou J, Mulhern D, Wang Y, Lee KA, Yang V, Aguiar M, Kornhauser J, Jia X, et al. (2014). Immunoaffinity enrichment and mass spectrometry analysis of protein methylation. Mol. Cell. Proteomics 13, 372–387. 10.1074/mcp.O113.027870. [PubMed: 24129315]
8. Musiani D, Bok J, Massignani E, Wu L, Tabaglio T, Ippolito MR, Cuomo A, Ozbek U, Zorgati H, Ghoshdastider U, et al. (2019). Proteomics profiling of arginine methylation defines PRMT5 substrate specificity. Sci. Signal. 12, eaat8388. 10.1126/scisignal.aat8388. [PubMed: 30940768]
9. Barsyte-Lovejoy D (2023). Studying Protein Arginine Methylation: Approaches and Methods. J. Vis. Exp. 191, e64821. 10.3791/64821.
10. Massignani E, Giambruno R, Maniaci M, Nicosia L, Yadav A, Cuomo A, Raimondi F, and Bonaldi T (2022). ProMetheusDB: An In-Depth Analysis of the High-Quality Human Methyl-proteome. Mol. Cell. Proteomics 21, 100243. 10.1016/j.mcpro.2022.100243. [PubMed: 35577067]
11. Thandapani P, O'Connor TR, Bailey TL, and Richard S (2013). Defining the RGG/RG motif. Mol. Cell. 50, 613–623. 10.1016/j.molcel.2013.05.021. [PubMed: 23746349]
12. Bremang M, Cuomo A, Agresta AM, Stugiewicz M, Spadotto V, and Bonaldi T (2013). Mass spectrometry-based identification and characterisation of lysine and arginine methylation in the human proteome. Mol. Biosyst. 9, 2231–2247. 10.1039/c3mb00009e. [PubMed: 23748837]
13. Dhar S, Vemulapalli V, Patananan AN, Huang GL, Di Lorenzo A, Richard S, Comb MJ, Guo A, Clarke SG, and Bedford MT (2013). Loss of the major Type I arginine methyltransferase PRMT1 causes substrate scavenging by other PRMTs. Sci. Rep. 3, 1311. 10.1038/srep01311. [PubMed: 23419748]
14. Courchaine EM, Barentine AES, Straube K, Lee DR, Bewersdorf J, and Neugebauer KM (2021). DMA-tudor interaction modules control the specificity of in vivo condensates. Cell 184, 3612–3625.e17. 10.1016/j.cell.2021.05.008. [PubMed: 34115980]
15. Simcikova D, Gelles-Watnick S, and Neugebauer KM (2023). Tudor-dimethylarginine interactions: the condensed version. Trends Biochem. Sci. 48, 689–698. 10.1016/j.tibs.2023.04.003. [PubMed: 37156649]
16. Wang Y, and Bedford MT (2023). Effectors and effects of arginine methylation. Biochem. Soc. Trans. 51, 725–734. 10.1042/BST20221147. [PubMed: 37013969]
17. Shanle EK, Shinsky SA, Bridgers JB, Bae N, Sagum C, Krajewski K, Rothbart SB, Bedford MT, and Strahl BD (2017). Histone peptide microarray screen of chromo and Tudor domains defines new histone lysine methylation interactions. Epigenet. Chromatin 10, 12. 10.1186/s13072-017-0117-5.
18. Liu H, Wang JYS, Huang Y, Li Z, Gong W, Lehmann R, and Xu RM (2010). Structural basis for methylarginine-dependent recognition of Aubergine by Tudor. Genes Dev. 24, 1876–1881. 10.1101/gad.1956010. [PubMed: 20713507]
19. Kim J, Daniel J, Espejo A, Lake A, Krishna M, Xia L, Zhang Y, and Bedford MT (2006). Tudor, MBT and chromo domains gauge the degree of lysine methylation. EMBO Rep. 7, 397–403. 10.1038/sj.embor.7400625. [PubMed: 16415788]
20. Jain K, Fraser CS, Marunde MR, Parker MM, Sagum C, Burg JM, Hall N, Popova IK, Rodriguez KL, Vaidya A, et al. (2020). Characterization of the plant homeodomain (PHD) reader family for their histone tail interactions. Epigenet. Chromatin 13, 3. 10.1186/s13072-020-0328-z.
21. Yang D, Nakao M, Shichijo S, Sasatomi T, Takasu H, Matsumoto H, Mori K, Hayashi A, Yamana H, Shirouzu K, and Itoh K (1999). Identification of a gene coding for a protein possessing shared tumor epitopes capable of inducing HLA-A24-restricted cytotoxic T lymphocytes in cancer patients. Cancer Res. 59, 4056–4063. [PubMed: 10463607]
22. Stanek D, Rader SD, Klingauf M, and Neugebauer KM (2003). Targeting of U4/U6 small nuclear RNP assembly factor SART3/p110 to Cajal bodies. J. Cell Biol. 160, 505–516. 10.1083/jcb.200210087. [PubMed: 12578909]
23. Klimesova K, Petrzilkova H, Barinka C, and Stanek D (2023). SART3 associates with a post-splicing complex. J. Cell Sci. 136, jcs260380. 10.1242/jcs.260380. [PubMed: 36620952]

24. Timani KA, Liu Y, and He JJ (2013). Tip110 interacts with YB-1 and regulates each other's function. BMC Mol. Biol. 14, 14. 10.1186/1471-2199-14-14.
25. Liu Y, Kim BO, Kao C, Jung C, Dalton JT, and He JJ (2004). Tip110, the human immunodeficiency virus type 1 (HIV-1) Tat-interacting protein of 110 kDa as a negative regulator of androgen receptor (AR) transcriptional activation. J. Biol. Chem. 279, 21766–21773. 10.1074/jbc.M314321200. [PubMed: 15031286]
26. Zhao W, Liu Y, Timani KA, and He JJ (2014). Tip110 protein binds to unphosphorylated RNA polymerase II and promotes its phosphorylation and HIV-1 long terminal repeat transcription. J. Biol. Chem. 289, 190–202. 10.1074/jbc.M113.529784. [PubMed: 24217245]
27. Long L, Thelen JP, Furgason M, Haj-Yahya M, Brik A, Cheng D, Peng J, and Yao T (2014). The U4/U6 recycling factor SART3 has histone chaperone activity and associates with USP15 to regulate H2B deubiquitination. J. Biol. Chem. 289, 8916–8930. 10.1074/jbc.M114.551754. [PubMed: 24526689]
28. Whitmill A, Timani KA, Liu Y, and He JJ (2016). Tip110: Physical properties, primary structure, and biological functions. Life Sci. 149, 79–95. 10.1016/j.lfs.2016.02.062. [PubMed: 26896687]
29. Park JK, Das T, Song EJ, and Kim EE (2016). Structural basis for recruiting and shuttling of the spliceosomal deubiquitinase USP4 by SART3. Nucleic Acids Res. 44, 5424–5437. 10.1093/nar/gkw218. [PubMed: 27060135]
30. Gao G, Hausmann S, Flores NM, Benitez AM, Shen J, Yang X, Person MD, Gayatri S, Cheng D, Lu Y, et al. (2023). The NFIB/CARM1 partnership is a driver in preclinical models of small cell lung cancer. Nat. Commun. 14, 363. 10.1038/s41467-023-35864-y. [PubMed: 36690626]
31. Lin CH, Huang HM, Hsieh M, Pollard KM, and Li C (2002). Arginine methylation of recombinant murine fibrillarin by protein arginine methyltransferase. J. Protein Chem. 21, 447–453. 10.1023/a:1021394903025. [PubMed: 12523648]
32. Denman RB (2002). Methylation of the arginine-glycine-rich region in the fragile X mental retardation protein FMRP differentially affects RNA binding. Cell. Mol. Biol. Lett. 7, 877–883. [PubMed: 12378270]
33. Eram MS, Shen Y, Szewczyk M, Wu H, Senisterra G, Li F, Butler KV, Kaniskan HÜ, Speed BA, Dela Seña C, et al. (2016). A Potent, Selective, and Cell-Active Inhibitor of Human Type I Protein Arginine Methyltransferases. ACS Chem. Biol. 11, 772–781. 10.1021/acschembio.5b00839. [PubMed: 26598975]
34. Nakayama K, Szewczyk MM, Dela Sena C, Wu H, Dong A, Zeng H, Li F, de Freitas RF, Eram MS, Schapira M, et al. (2018). TP-064, a potent and selective small molecule inhibitor of PRMT4 for multiple myeloma. Oncotarget 9, 18480–18493. 10.18632/oncotarget.24883. [PubMed: 29719619]
35. Chan-Penebre E, Kuplast KG, Majer CR, Boriack-Sjodin PA, Wigle TJ, Johnston LD, Rioux N, Munchhof MJ, Jin L, Jacques SL, et al. (2015). A selective inhibitor of PRMT5 with in vivo and in vitro potency in MCL models. Nat. Chem. Biol. 11, 432–437. 10.1038/nchembio.1810. [PubMed: 25915199]
36. Novotny I, Malinova A, Stejskalova E, Mateju D, Klimesova K, Roithova A, Sveda M, Knejzlik Z, and Stanek D (2015). SART3-Dependent Accumulation of Incomplete Spliceosomal snRNPs in Cajal Bodies. Cell Rep. 10, 429–440. 10.1016/j.celrep.2014.12.030. [PubMed: 25600876]
37. Tucker KE, Berciano MT, Jacobs EY, LePage DF, Shpargel KB, Rossire JJ, Chan EK, Lafarga M, Conlon RA, and Matera AG (2001). Residual Cajal bodies in coilin knockout mice fail to recruit Sm snRNPs and SMN, the spinal muscular atrophy gene product. J. Cell Biol. 154, 293–307. 10.1083/jcb.200104083. [PubMed: 11470819]
38. Branscombe TL, Frankel A, Lee JH, Cook JR, Yang Z, Pestka S, and Clarke S (2001). PRMT5 (Janus kinase-binding protein 1) catalyzes the formation of symmetric dimethylarginine residues in proteins. J. Biol. Chem. 276, 32971–32976. 10.1074/jbc.M105412200. [PubMed: 11413150]
39. Ratovitski T, Arbez N, Stewart JC, Chighladze E, and Ross CA (2015). PRMT5-mediated symmetric arginine dimethylation is attenuated by mutant huntingtin and is impaired in Huntington's disease (HD). Cell Cycle 14, 1716–1729. 10.1080/15384101.2015.1033595. [PubMed: 25927346]

40. Kim H, Barua A, Huang L, Zhou T, Bolaji M, Zachariah S, Mitra A, Jung SY, He B, and Feng Q (2023). The cancer testis antigen TDRD1 regulates prostate cancer proliferation by associating with the snRNP biogenesis machinery. Oncogene 42, 1821–1831. 10.1038/s41388-023-02690-x. [PubMed: 37041411]
41. Huttlin EL, Bruckner RJ, Navarrete-Perea J, Cannon JR, Baltier K, Gebreab F, Gygi MP, Thornock A, Zarraga G, Tam S, et al. (2021). Dual proteome-scale networks reveal cell-specific remodeling of the human interactome. Cell 184, 3022–3040.e28. 10.1016/j.cell.2021.04.011. [PubMed: 33961781]
42. Hock J, Weinmann L, Ender C, Rudel S, Kremmer E, Raabe M, Urlaub H, and Meister G (2007). Proteomic and functional analysis of Argonaute-containing mRNA-protein complexes in human cells. EMBO Rep. 8, 1052–1060. 10.1038/sj.embor.7401088. [PubMed: 17932509]
43. Zhang Q, Harding R, Hou F, Dong A, Walker JR, Bteich J, and Tong Y (2016). Structural Basis of the Recruitment of Ubiquitin-specific Protease USP15 by Spliceosome Recycling Factor SART3. J. Biol. Chem. 291, 17283–17292. 10.1074/jbc.M116.740787. [PubMed: 27255711]
44. Shen S, Park JW, Lu ZX, Lin L, Henry MD, Wu YN, Zhou Q, and Xing Y (2014). rMATS: robust and flexible detection of differential alternative splicing from replicate RNA-Seq data. Proc. Natl. Acad. Sci. USA 111, E5593–E5601. 10.1073/pnas.1419161111. [PubMed: 25480548]
45. Friesen WJ, Paushkin S, Wyce A, Massenet S, Pesiridis GS, Van Duyne G, Rappsilber J, Mann M, and Dreyfuss G (2001). The methylosome, a 20S complex containing JBP1 and pICln, produces dimethylarginine-modified Sm proteins. Mol. Cell Biol. 21, 8289–8300. 10.1128/MCB.21.24.8289-8300.2001. [PubMed: 11713266]
46. Meister G, Eggert C, Bühler D, Brahms H, Kambach C, and Fischer U (2001). Methylation of Sm proteins by a complex containing PRMT5 and the putative U snRNP assembly factor pICln. Curr. Biol. 11, 1990–1994. 10.1016/s0960-9822(01)00592-9. [PubMed: 11747828]
47. Meister G, and Fischer U (2002). Assisted RNP assembly: SMN and PRMT5 complexes cooperate in the formation of spliceosomal UsnRNPs. EMBO J. 21, 5853–5863. 10.1093/emboj/cdf585. [PubMed: 12411503]
48. Tripsianes K, Madl T, Machyna M, Fessas D, Englbrecht C, Fischer U, Neugebauer KM, and Sattler M (2011). Structural basis for dimethylarginine recognition by the Tudor domains of human SMN and SPF30 proteins. Nat. Struct. Mol. Biol. 18, 1414–1420. 10.1038/nsmb.2185. [PubMed: 22101937]
49. Enders L, Siklos M, Borggräfe J, Gaussmann S, Koren A, Malik M, Tomek T, Schuster M, Reiniš J, Hahn E, et al. (2023). Pharmacological perturbation of the phase-separating protein SMNDC1. Nat. Commun. 14, 4504. 10.1038/s41467-023-40124-0. [PubMed: 37587144]
50. Machyna M, Neugebauer KM, and Staněk D (2015). Coilin: The first 25 years. RNA Biol. 12, 590–596. 10.1080/15476286.2015.1034923. [PubMed: 25970135]
51. Hebert MD, Shpargel KB, Ospina JK, Tucker KE, and Matera AG (2002). Coilin methylation regulates nuclear body formation. Dev. Cell 3, 329–337. 10.1016/s1534-5807(02)00222-8. [PubMed: 12361597]
52. D'Andrea LD, and Regan L (2003). TPR proteins: the versatile helix. Trends Biochem. Sci. 28, 655–662. 10.1016/j.tibs.2003.10.007. [PubMed: 14659697]
53. Preker PJ, and Keller W (1998). The HAT helix, a repetitive motif implicated in RNA processing. Trends Biochem. Sci. 23, 15–16. 10.1016/s0968-0004(97)01156-0. [PubMed: 9478129]
54. Champion EA, Kundrat L, Regan L, and Baserga SJ (2009). A structural model for the HAT domain of Utp6 incorporating bioinformatics and genetics. Protein Eng. Des. Sel. 22, 431–439. 10.1093/protein/gzp022. [PubMed: 19515729]
55. Horton JR, Zhou J, Chen Q, Zhang X, Bedford MT, and Cheng X (2023). A complete methyl-lysine binding aromatic cage constructed by two domains of PHF2. J. Biol. Chem. 299, 102862. 10.1016/j.jbc.2022.102862. [PubMed: 36596360]
56. Katz Y, Wang ET, Airoldi EM, and Burge CB (2010). Analysis and design of RNA sequencing experiments for identifying isoform regulation. Nat. Methods 7, 1009–1015. 10.1038/nmeth.1528. [PubMed: 21057496]

57. Wang ET, Sandberg R, Luo S, Khrebtukova I, Zhang L, Mayr C, Kingsmore SF, Schroth GP, and Burge CB (2008). Alternative isoform regulation in human tissue transcriptomes. Nature 456, 470–476. 10.1038/nature07509. [PubMed: 18978772]

Highlights

- SART3 is a methylarginine reader
- The HAT repeat domain of SART3 harbors reader function
- Reader activity is implicated in the regulation of RNA splicing

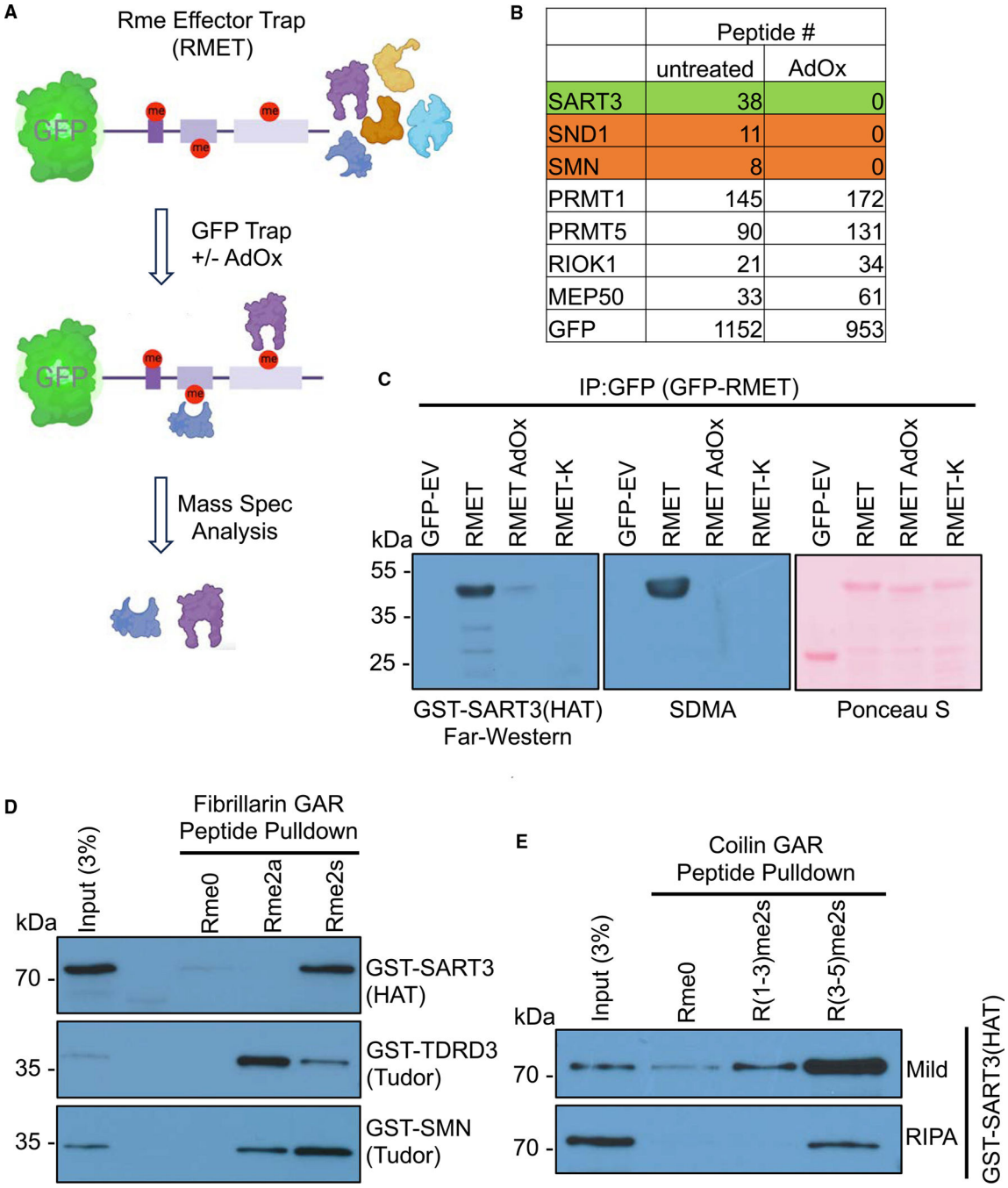

Figure 1. The HAT repeats of SART3 read SDMA-marked GAR motifs

(A) Schematic representation of the GFP-Trap-based IP-mass spectrometry (MS) approach. (B) List of GFP-RMET interacting proteins identified by IP-MS. HEK293T cells were transfected with GFP-RMET, and half the cells were treated with AdOx for 3 days and subjected to IP-MS analysis. The number of peptides identified for each protein is listed. (C) Far-western analysis of the interaction between a GST-SART3(HAT) and RMET. HEK293T cells were transfected with GFP-EV (empty vector) or the GFP-RMET fusion.

After a 3-day treatment with AdOx, total lysates were probed with GST-SART3(HAT) and detected with anti-GST antibody.

(D) GST-SART3(HAT) pull-downs using biotinylated fibrillarin GAR peptides. GST-TDRD3(Tudor) and GST-SMN(Tudor) are controls. A mild buffer (150 mM NaCl) was used.

(E) GST-SART3(HAT) pull-downs using biotinylated coilin GAR peptides and using mild buffer (300 mM NaCl) and RIPA.

Experiments (C–E) were independently repeated three times, with similar results.

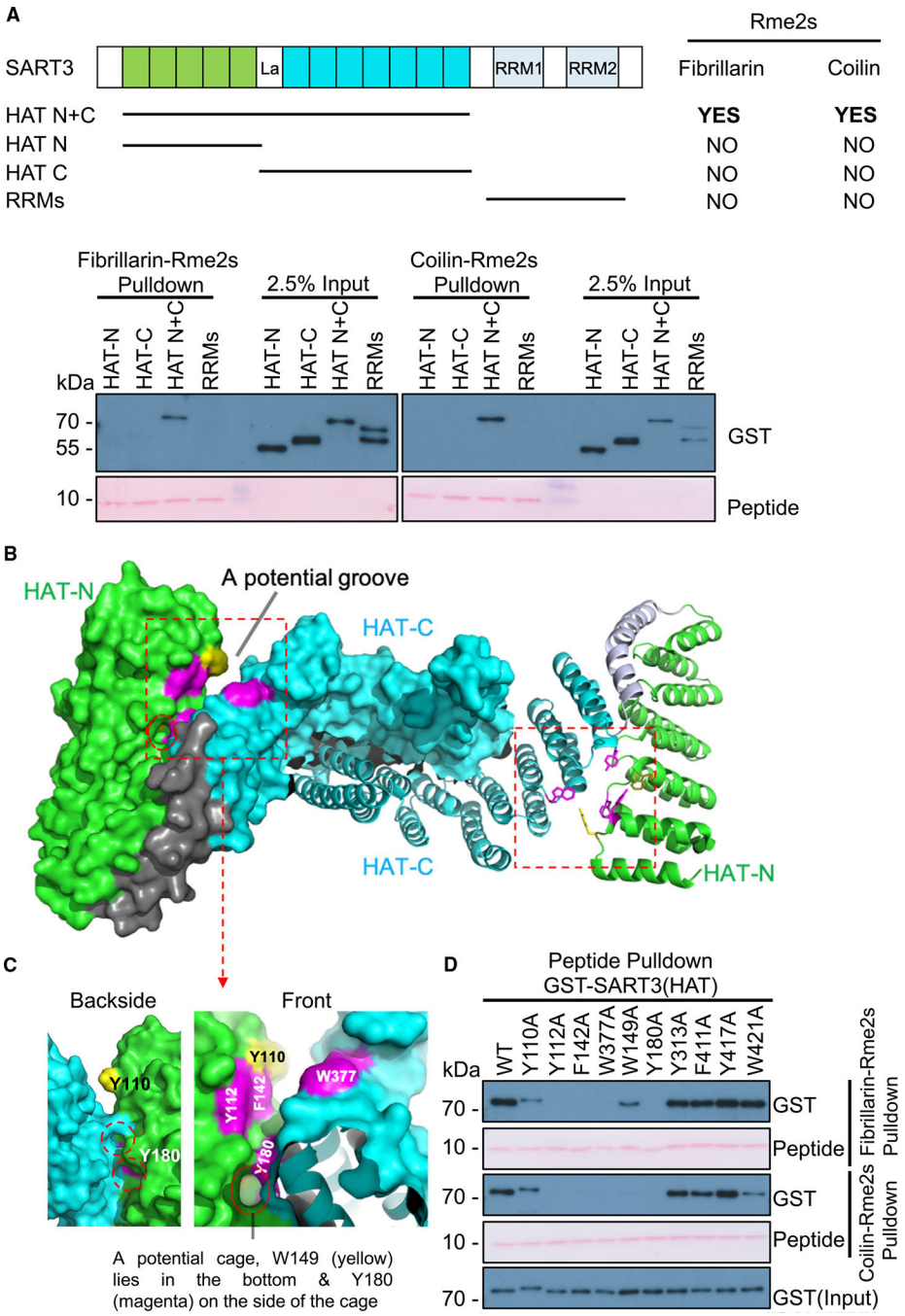

Figure 2. Structure-function studies detailing the methyl-reader properties of SART3

(A) Graphic depiction of the regions of SART3 used in the peptide pull-down assays with the results of the interaction mapping. Western analysis of the pull-downs with respective methylated peptides. Ponceau-S staining was performed for peptide loading.

(B) A potential groove is formed by SART3 HAT-N and HAT-C repeats. The aromatic residues around this groove are highlighted in pink/yellow. The N- (green) and C-terminal (teal) HAT repeats of SART3 are split by a La/SSB binding region (gray). SART3 homodimerize via HAT-C.

(C) Two opposite views of a potential aromatic groove that is formed by several key residues in the SART3 HAT repeats. The marked aromatic residues within this groove are critical for the methyl-peptide interactions shown in (D).

(D) Peptide pull-downs using the wild-type (WT) SART3 HAT repeats harboring the indicated point mutants. Ponceau-S staining was performed for the peptide loading. Experiments (A and D) were independently repeated three times, with similar results.

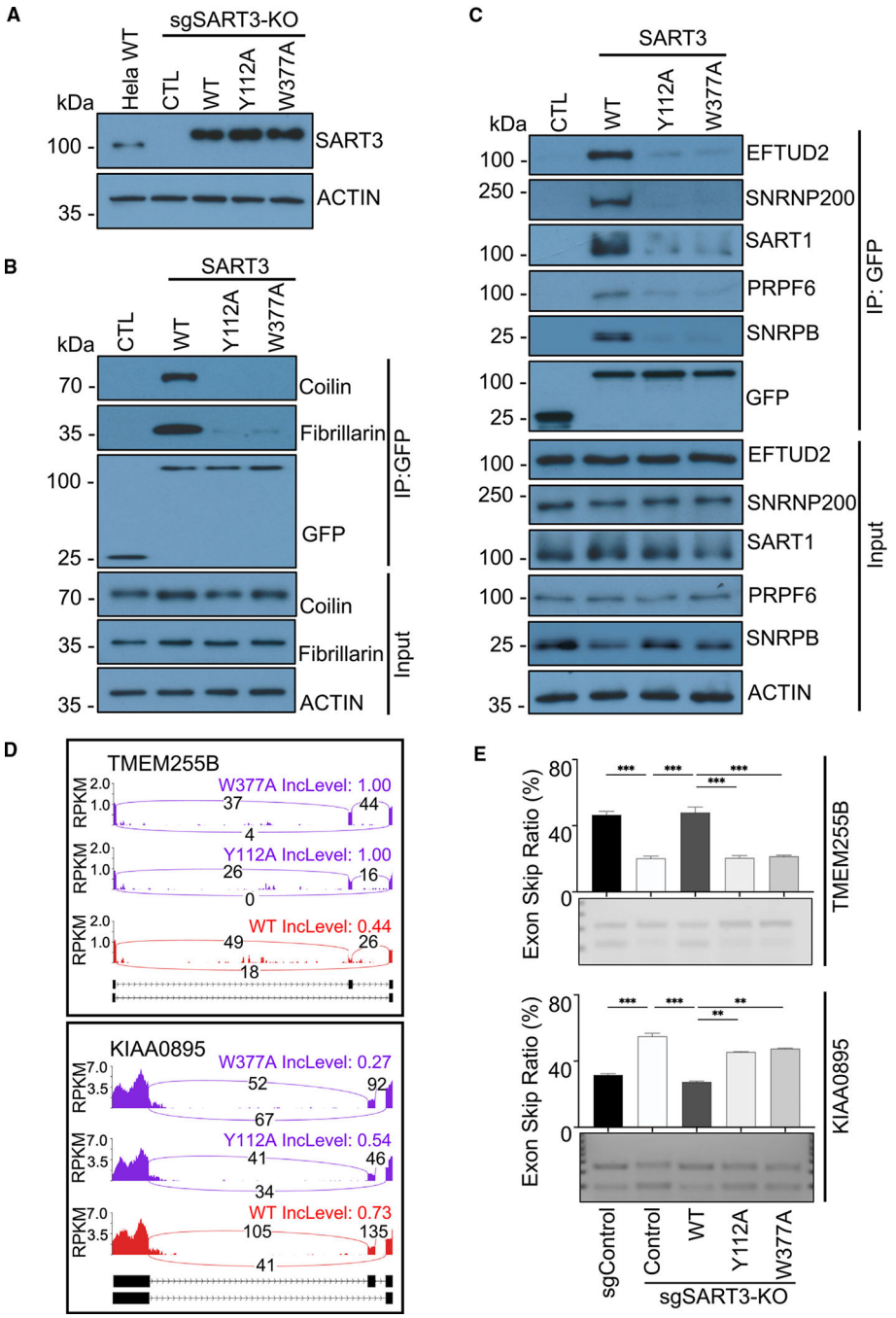

Figure 3. The methyl-reader activity of SART3 is required for efficient RNA splicing

(A) Western blot analysis of SART3 expression in CRISPR-mediated SART3-knockout (KO) HeLa cells and the stable restoration with GFP fusions to WT and mutant (Y112A and W377A) SART3.

(B) IP/western blot analysis of the SART3 interaction with coilin and fibrillarin. Restored HeLa SART3-KO cells in (A) were used.

(C) IP/western blot validation of the interaction between SART3 and a subset of spliceosome proteins identified by IP-MS. Restored HeLa SART3-KO cells in (A) were used.

(D) Sashimi plots depicting exon skipping in the representative genes TMEM255B and KIAA0895 in HeLa SART3-KO cells restored with WT (red) and mutant (purple) SART3. False discovery rate < 0.05.

(E) Semiquantitative RT-PCR supporting the *TMEM255B* and *KIAA0895* exon skipping analysis using HeLa control cells (endogenous SART3), SART3-KO control cells (no SART3), and HeLa sgSART3-KO cells restored with WT GFP-SART3 or the Y112A and W377A mutants (restored), as shown in (A). Three biological repeats were performed ($n = 3$). The PCR products were quantified by densitometric analysis, and the exon skipping ratio is shown in a percentage expressed as the mean ± SEM. Unpaired t test was used to calculate p values: $^{**}p < 0.01$ and $^{***}p < 0.001$.

KEY RESOURCES TABLE

REAGENT or RESOURCE	SOURCE	IDENTIFIER
Antibodies		
SART3	Bethyl	Cat# A301–521A; RRID: AB_999668
GFP (WB)	Santa Cruz Biotechnology	Cat# sc-9996; RRID: AB_627695
GFP (IP)	Invitrogen	Cat# A6455; RRID: AB_2314549
GST	This paper	N/A
Fibrillarin	Proteintech	Cat# 16021–1-AP; RRID: AB_2105788
Coilin	Cell Signaling Technology	Cat# 14168; RRID: AB_2798410
Actin	Sigma-Aldrich	Cat# A1978; RRID: AB_476692
PABP(ADMA)	Cell Signaling Technology	Cat# 3505; RRID: AB_2298971
FAM(ADMA)	In house	N/A
ADMA	In house	N/A
SDMA	In house	N/A
MMA	In house	N/A
PRMT1	Bethyl	Cat# A300–722A; RRID: AB_533421
PRMT5	Active Motif	Cat# 61001
SND1	Bethyl	Cat# A302–883A; RRID: AB_10631268
SMN	Bethyl	Cat# A301–862A; RRID: AB_1309784
EFTUD2	Proteintech	Cat# 10208–1-AP; RRID: AB_2095834
SNRNP200	Proteintech	Cat# 23875–1-AP; RRID: AB_2879346
SART1	Proteintech	Cat# 22675–1-AP; RRID: AB_2879148
PRPF6	Proteintech	Cat# 23929–1-AP; RRID: AB_2879365
AGO1	Cell Signaling Technology	Cat# 5053; RRID: AB_2616013
SNRPB	Santa Cruz Biotechnology	Cat# sc-271094; RRID: AB_10611786
La	Bethyl	Cat# A303–902A; RRID: AB_2620252
USP4	Bethyl	Cat# A300–829A; RRID: AB_597888
USP15	Bethyl	Cat# A300–923A; RRID: AB_2214726
Peroxidase AffiniPure Donkey Anti-Mouse IgG	Jackson ImmunoResearch	Cat# 715–035-151; RRID: AB_2340771
Peroxidase AffiniPure Donkey Anti-Rabbit IgG	Jackson ImmunoResearch	Cat# 711–035-152; RRID: AB_10015282

REAGENT or RESOURCE	SOURCE	IDENTIFIER
Fibrillarin peptide Rme0 (unmethylated) GGRGRGGGFRGRGRGGGG-Biotin	CPC Scientific	N/A
Fibrillarin peptide Rme2a (ADMA) GG[Rme2a]G[Rme2a]GGGF[Rme2a] G[Rme2a]G[Rme2a]GGGG-Biotin	CPC Scientific	N/A
Fibrillarin peptide Rme2s (SDMA) GG[Rme2s]G[Rme2s]GGGF[Rme2s] G[Rme2s]G[Rme2s]GGGG-Biotin	CPC Scientific	N/A
Coilin peptide Rme0 (unmethylated) Biotin-AKGRGMRGRGRGRGHP-Amide	Vivitide	N/A
Coilin peptide R(1–3)me2s (SDMA) BiotinAKG[Rme2s]GM[Rme2s] G[Rme2s]GRGRGHP-Amide	Vivitide	N/A
Coilin peptide R(3–5)me2s (SDMA) BiotinAKGRGMRG[Rme2s]G[Rme2s] G[Rme2s]GHP-Amide	Vivitide	N/A
Critical commercial assays		
QIAprep Spin Miniprep Kit	QIAGEN	Cat# 27106
RNeasy Mini Kit	Qiagen	Cat# 74106
Q5 High-Fidelity 2X Master Mix	NEB	Cat# M0492
Q5 Site-directed mutagenesis kit	NEB	Cat# E0554S
Superscript first-strand synthesis kit	Invitrogen	Cat# 18091050
iTaq Universal SYBR Green Supermix	Bio-Rad	Cat# 1725121
iScript cDNA synthesis Kit	Bio-Rad	Cat# 1708891
Deposited data		
RNA-seq	This paper	GEO accession: GSE246489
IP-MS data	This paper	PRIDE accession: Experimental models: Cell lines
Human: HeLa	ATCC	Cat# CCL2; RRID: CVCL_0030
Human: HEK293T	ATCC	Cat# CRL-1573; RRID: CVCL_0045
Human: HeLa-SART3 knockout	This paper	N/A
Oligonucleotides		
See Table S4 for Oligonucleotides with sequences		N/A

REAGENT or RESOURCE	SOURCE	IDENTIFIER
Recombinant DNA		
Plasmid: psPAX2	Trono Lab	Cat# Addgene #12260; RRID: Addgene_12260
Plasmid: pMD2.G	Trono Lab	Cat# Addgene #12259; RRID: Addgene_12259
Plasmid: LentiCRISPR v2-Blast	Zhang Lab	Cat# Addgene #83480; RRID: Addgene_83480
Plasmid: GFP-RMET(R)	Biomatik	N/A
Plasmid: GFP-RMET(K)	Biomatik	N/A
Plasmid: GST-SMN(TUDOR)	Biomatik	N/A
Plasmid: GST-TDRD3(TUDOR)	Biomatik	N/A
Plasmid: GST-SART3(HAT)	This paper	N/A
Plasmid: GST-SART3(HAT-N)	This paper	N/A
Plasmid: GST-SART3(HAT-C)	This paper	N/A
Plasmid: GST-SART3(RRMs)	This paper	N/A
Plasmid: GST-SART3(HAT Y110A)	This paper	N/A
Plasmid: GST-SART3(HAT Y112A)	This paper	N/A
Plasmid: GST-SART3(HAT F142A)	This paper	N/A
Plasmid: GST-SART3(HAT W377A)	This paper	N/A
Plasmid: GST-SART3(HAT W149A)	This paper	N/A
Plasmid: GST-SART3(HAT Y180A)	This paper	N/A
Plasmid: GST-SART3(HAT Y313A)	This paper	N/A
Plasmid: GST-SART3(HAT F411A)	This paper	N/A
Plasmid: GST-SART3(HAT Y417A)	This paper	N/A
Plasmid: GST-SART3(HAT W421A)	This paper	N/A
Plasmid: GST-SART3(HAT F411A)	This paper	N/A
Plasmid: GFP-SART3	Biomatik	N/A
Plasmid: GFP-SART3 Y112A	This paper	N/A
Plasmid: GFP-SART3 F142A	This paper	N/A
Plasmid: GFP-SART3 Y180A	This paper	N/A
Plasmid: GFP-SART3 W377A	This paper	N/A
Plasmid: Lenti-Puro-GFP EV	This paper	N/A
Plasmid: Lenti-Puro-GFP-SART3	This paper	N/A

REAGENT or RESOURCE	SOURCE	IDENTIFIER
Plasmid: Lenti-Puro-GFP-SART3 Y112A	This paper	N/A
Plasmid: Lenti-Puro-GFP-SART3 F142A	This paper	N/A
Software and algorithms		
Prism 9	GraphPad	https://www.graphpad.com/
Scaffold 5	Proteome Software	https://www.proteomesoftware.com/products/scaffold-5
rmats2sashimiplot	GitHub	https://github.com/Xinglab/rmats2sashimiplot
AlphaFold	DeepMind	https://deepmind.google/technologies/alphafold/